Key Points:
- Gravity wave packets in the Venusian atmosphere were detected in radio occultation temperature profiles using wavelet transform
- The characteristics of quasi-monochromatic wave packets were studied in terms of the consistency with the saturation model
- Altitude and latitude dependences might be caused by radiative damping and the latitudinal variation of static stability, respectively

Correspondence to:
T. Imamura,
t_imamura@edu.k.u-tokyo.ac.jp

Gravity Wave Packets in the Venusian Atmosphere Observed by Radio Occultation Experiments: Comparison With Saturation Theory

Ryota Mori[1], Takeshi Imamura[1], Hiroki Ando[2], Bernd Häusler[3], Martin Pätzold[4], and Silvia Tellmann[4]

[1]Graduate School of Frontier Sciences, The University of Tokyo, Kashiwa, Japan, [2]Kyoto Sangyo University, Faculty of Science, Kyoto, Japan, [3]Universität der Bundeswehr München, Institut für Raumfahrttechnik und Weltraumnutzung, Neubiberg, Germany, [4]Abteilung Planetenforschung, Universität zu Köln, Rheinisches Institut für Umweltforschung, Cologne, Germany

Abstract The characteristics of gravity wave packets in the Venusian atmosphere were studied using high-vertical-resolution temperature profiles obtained by ESA's Venus Express and JAXA's Akatsuki radio occultation experiments with radio holographic methods. Localized disturbances were detected by applying a wavelet transform to the temperature profiles. The packet lengths were found to be distributed over 0.6–10 km, in which typically 1.5–4.0 oscillations are included. The number of oscillations per wave packet was found to have only a slight dependence on the wavelength, which is consistent with the −3 power law dependence of the spectral density on the wavenumber in the saturation model. The spectral densities of the wave packets are roughly aligned with the power law of the saturation model, while the saturation ratio for each quasi-monochromatic wave is low. This suggests that the saturated spectrum is produced by the superposition of individually unsaturated quasi-monochromatic waves. Waves with short vertical wavelengths (<1.5 km) were found to be more prevalent at lower altitudes than at higher altitudes, implying an effect of radiative damping during upward propagation. The amplitude was found to be larger at higher latitudes, which might be attributed to an increase in background static stability at high latitudes, which allows larger saturation amplitudes.

Plain Language Summary Although gravity waves are thought to play crucial roles in transporting momentum and energy in the Venusian atmosphere, their characteristics are not well constrained from observations. Here the characteristics of Venusian gravity waves were studied by extracting wave packets from temperature profiles obtained by radio occultation experiments using Venus orbiters. The number of oscillations per wave packet was found to have only a slight dependence on the wavelength. The observed amplitudes and the vertical wavenumber spectra suggest that the superposition of quasi-monochromatic waves causes convective instability to limit their amplitudes. The decrease of short vertical-scale waves with altitude is thought to be caused by radiative dampling, and the increase of the amplitude at high latitudes is attributed to an effect of the background static stability. The finding that the wave amplitude is mostly limited by convective instability serves as the basis for gravity wave parameterization in numerical models.

1. Introduction

Internal gravity waves play crucial roles in transporting momentum and energy in the Earth's atmosphere (e.g., Fritts & Alexander, 2003). In the Venusian atmosphere, wave trains with horizontal wavelengths of tens to hundreds of kilometers, indicative of gravity waves, have been observed as localized quasi-monochromatic wave packets in cloud and airglow images (e.g., Garcia et al., 2009; Peralta et al., 2008, 2019; Piccialli et al., 2014). Bow-like stationary features indicative of topographic gravity waves have been observed in cloud images (Fukuhara et al., 2017; Kitahara et al., 2019; Kouyama et al., 2017; Sato et al., 2020). Gravity wave-like features have also been detected by radio occultation observations. Hinson and Jenkins (1995) studied temperature oscillations with vertical wavelengths of several kilometers seen in Magellan radio occultation temperatures. They attributed the oscillations to vertically propagating gravity waves and suggested a major role for radiative damping in limiting the wave amplitude. They also suggested a contribution of

wave-induced drag to the decrease of the mean zonal wind speed with height above the clouds. Using the temperature profiles obtained by the Venus Express radio occultation, Tellmann et al. (2012) studied the meridional distribution of temperature fluctuations with vertical wavelengths of <4 km that can be attributed to gravity waves. They reported an increase in the wave activity with increasing latitude, suggesting wave generation near the high-latitude jets. Imamura et al. (2014) argued that wave generation by cloud-level convection, which might be stronger at higher latitudes due to stronger radiative cooling of the cloud top, can also explain the observed latitude dependence. Gravity wave-like perturbations were also observed in situ by Pioneer Venus probes and orbiters (Seiff et al., 1992) and by Vega balloons (Ingersoll et al., 1987). Numerical models suggest that gravity waves play crucial roles in shaping the planetary-scale wind structure (Hoshino et al., 2013; Hou & Farrell, 1987; Schubert & Walterscheid, 1984; Zalucha et al., 2013).

The interaction of gravity waves with the mean flow occurs due to the nonlinearity of the waves, which is usually measured by the ratio of the amplitude to the saturation amplitude. The basic idea of saturation is that the wave perturbation causes the total lapse rate to become superadiabatic, leading to convective mixing and attenuation of the wave to the convective instability threshold (e.g., Lindzen, 1981). This is not caused by a single wave, but by a superposition of quasi-monochromatic wave packets of all wavenumbers jointly achieving a state of convective instability (Smith et al., 1987). Based on this concept, a model for the vertical wavenumber spectrum of saturated waves was developed. The saturation model gives the spectral density $F_{T'/\bar{T}}$ of the fractional temperature disturbance $T'/\bar{T}$, where T' is the temperature disturbance and $\bar{T}$ is the background temperature, as (Smith et al., 1987; Tsuda & Hocke, 2002; Tsuda et al., 1991):

$$F_{T'/\bar{T}} = \frac{1}{4\pi^2} \frac{N^4}{10g^2 k_z^3},\tag{1}$$

where N is the Brunt-Väisälä frequency, g is the gravitational acceleration, and $k_z = 1/\lambda_z$ is the vertical wavenumber, with λ_z being the vertical wavelength. The use of cycles per unit length instead of radians per unit length in the definition of the wavenumber is the convention in plots of vertical wavenumber spectra. The k_z^{-3} dependence relies on the assumption that the bandwidth of each quasi-monochromatic wave is proportional to the local wavenumber (Dewan & Good, 1986; Smith et al., 1987). This is equivalent to a condition that the number of wave cycles in each quasi-monochromatic wave packet is independent of the wavenumber. The saturated spectral density given by (Equation 1) is a factor of 3 times smaller than that obtained by assuming that individual wave packets are saturated in isolation. The saturation model agrees well with observations of the Earth's middle atmosphere (e.g., Fritts & Alexander, 2003; Smith et al., 1987; Tsuda & Hocke, 2002; Tsuda et al., 1989, 1991).

Ando et al. (2015) studied the vertical wavenumber spectra of the temperature profiles of the Venusian atmosphere obtained by the Venus Express radio occultation and showed that the spectra above ~65 km altitude are largely consistent with the saturation model at wavelengths of 1–5 km. At shorter wavelengths the vertical resolution limits the analysis. From the characteristics of saturated waves, wave-driven turbulent diffusion coefficients were estimated. They also determined the amplitude growth with height of unsaturated waves ($\lambda_z > 5$ km). Though neutral stability layers indicative of saturation were rarely observed in the temperature profiles Ando et al. (2015) used, Imamura et al. (2018) showed that thin near-neutral layers frequently exist in the Venusian atmosphere, using high-vertical-resolution temperature profiles obtained by a radio holographic method from the Venus Express and Akatsuki radio occultation experiments. Examples of the vertical profile of the static stability $S = dT/dz + g/C_p$ are shown in Figure 1, where dT/dz is the vertical gradient of the temperature, g is the gravitational acceleration and C_p is the specific heat at constant pressure given by Seiff et al. (1985). Thin layers of near-neutral stability are distributed over a wide range of latitudes and altitudes. Imamura et al. (2018) also found that the vertical wavenumber spectrum roughly follows the saturation model down to wavelengths of a few hundreds of meters. The characteristics of quasi-monochromatic wave packets and their contributions to the saturated spectrum in the Venusian atmosphere are still unknown.

Here, we study the characteristics of gravity wave packets in the Venusian atmosphere using high-vertical-resolution temperature profiles obtained by applying a radio holographic method to the Venus Express and Akatsuki radio occultation data (Imamura et al., 2018). A wavelet transform is applied to Venusian temperature profiles for the first time. Wavelet transform has been used in studies of Earth's gravity waves (Sato & Yamada, 1994; Shimomai et al., 1996) and Saturn's gravity waves (Harrington et al., 2010). In the present
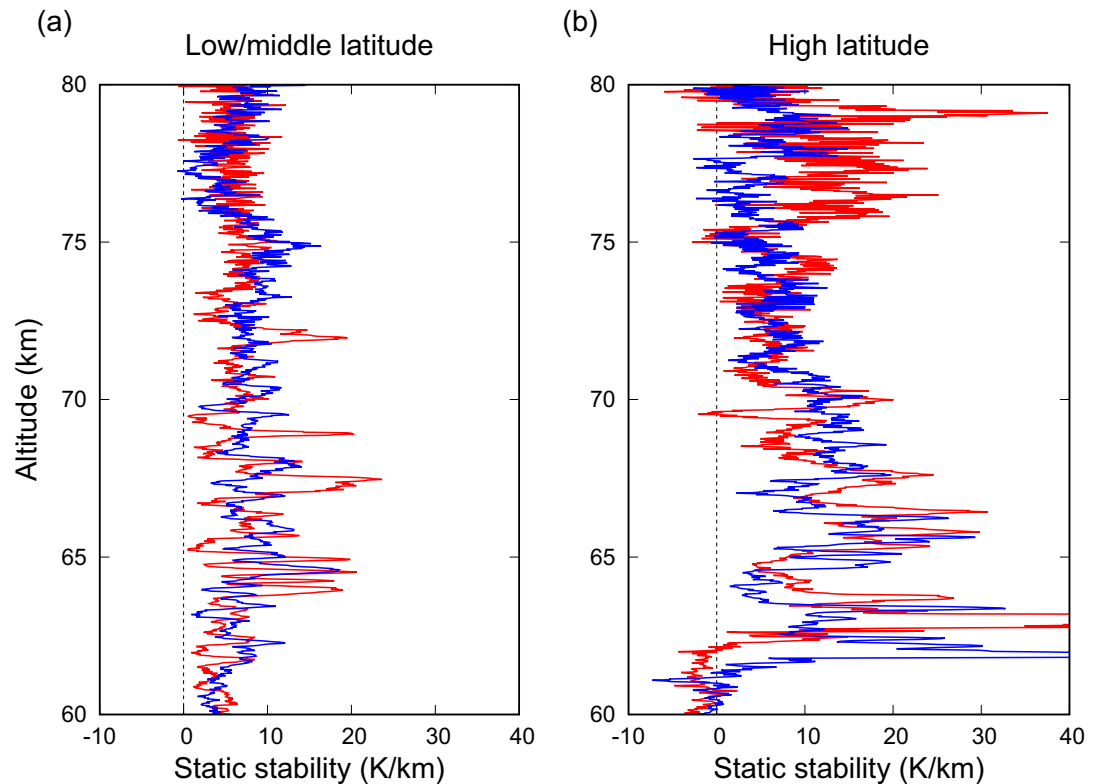
Figure 1. Examples of the vertical profile of the static stability obtained by a radio holographic analysis (Imamura et al., 2018). The data were obtained by Akatsuki's entry occultation on May 26, 2017 at a latitude of ∼0.4°S (a, red), Akatsuki's exit occultation on June 6, 2017 at a latitude of ∼38.9°S (a, blue), Akatsuki's exit occultation on March 3, 2016 at a latitude of ∼66.9°S (b, red), and Venus Express's entry occultation on July 31, 2017 at a latitude of ∼73.3°S (b, blue). The error in the static stability is typically <0.7 K km^{-1} at altitudes lower than 75 km.

study, the amplitudes and packet lengths of individual quasi-monochromatic waves and their contribution to saturation are investigated. Combined with the altitude and latitude dependences, the dissipation processes of the waves are discussed. Section 2 describes the data set and the analysis procedure, Section 3 gives the results, and Section 4 provides a discussion and conclusions.

2. Data Set and Analysis Procedure

2.1. Temperature Profiles

The radio occultation temperatures we analyzed are those retrieved by Imamura et al. (2018). The raw data were obtained by the Radio Science experiment (VeRa) (Tellmann et al., 2009, 2012) on ESA's Venus Express (Svedhem et al., 2007) and the Radio Science (RS) (Imamura et al., 2017, 2018) on JAXA's Akatsuki (Nakamura et al., 2011, 2016). From the whole data set of VeRa, we analyzed 32 occultation experiments distributed evenly in latitude and local time taken during the period from July 2006 to September 2009. These data are a subset of the data used by Tellmann et al. (2012). Akatsuki RS started in March 2016. We analyzed 27 occultation experiments conducted during the period from March 2016 to July 2017 at the Usuda Deep Space Center (UDSC) of JAXA. Using data from the two missions that are separated by ∼10 years from each other allows us to investigate possible long-term variations.

Imamura et al. (2018) have processed the raw VeRa and Akatsuki RS data using full spectrum inversion (FSI) (Jensen et al., 2003; Tsuda et al., 2011), which is one of the radio holographic methods, to achieve vertical resolutions of ∼150 m. This method is different from the conventional geometrical optics method used in Tellmann et al. (2009, 2012) and Imamura et al. (2017), in which the vertical resolution is determined by the Fresnel diameter, which is typically 400–700 m (Ando et al., 2015; Häusler et al., 2006;

Imamura et al., 2017). FSI can decipher multipath propagation that frequently occurs in radio occultation of the Venusian atmosphere. The vertical grid interval of the temperature profiles is taken to be 10 m. The observation points used are widely distributed in space and local time (see Figure 2 in Imamura et al., 2018).

2.2. Identifying Wave Packets

Localized waves were extracted using a wavelet transform, which has been applied to various geophysical and astrophysical data including gravity waves in the Earth's atmosphere. The wavelet transform was performed using the Python module PyCWT, based on Torrence and Compo (1998). The Morlet function was used as the wavelet basis function. The analysis procedure is described below.

Temperature profiles spanning the altitude region of 60–80 km were analyzed. Before applying the wavelet transform, short vertical wavelength (<4 km) components were extracted by subtracting a smoothed profile from the original profile for each observation. Smoothing was done by calculating the running average with an averaging width of 4 km using the Python routine numpy.convolve in the NumPy module. The wavelet transform was applied to the residual highpass-filtered profiles. An example of the processing procedure is shown in Figure 2. The altitude is the radial distance from the surface of Venus, which is located at a radius of 6,051.8 km. This definition is used throughout the study. In this temperature profile, a vertical temperature gradient close to the adiabatic lapse rate is seen at 67–68 km altitudes, indicating occurrence of wave saturation. The vertical wavenumber k_z against which the wavelet spectrum is plotted is the inverse of the vertical wavelength without a 2π factor. The 90% confidence level shown in the wavelet spectrum was calculated following the method of Torrence and Compo (1998). The hatched regions represent the cone of influence (COI), in which the results are less reliable because of the influence of the boundaries.

The local maxima in the wavelet spectrum outside the COI are candidates for wave packets. The cross sections that traverse the two local maxima in the wavelet spectrum (Figure 2c) are shown in Figure 2d. The packet length is defined as the full width at half maximum of each peak along the altitude (red arrow in Figure 2d). When either of the half maximum points is within the COI, the packet length is obtained as twice the half width at half maximum on the side that does not overlap with the COI (purple arrow in Figure 2d). The peak is not considered to be a wave packet when both of the half maximum points are within the COI. We also define the following criteria for wave packets.

1. The power exceeds the 90% confidence level everywhere between the peak and the half maximum points along the altitude.
2. The wavelength exceeds 0.5 km considering the vertical resolution.
3. There are no other local maxima that have values exceeding the peak of interest within $\pm 0.5\lambda_z$ in the altitude direction and $k_z/1.2$–$1.2k_z$ in the wavenumber direction.
4. The background static stability, which is the value obtained by the 4 km-width running average, is positive within the wave packet.

The wave packets indicated by dots in Figure 2c satisfy the criteria above.

2.3. Spectral Density and Amplitude

The wavelet transform of a temperature disturbance profile gives the peak spectral density $F_{T'}$ in units of K^2 km^{-1}. The quantity used in later analysis is the peak spectral density of the fractional temperature disturbance $T'/\overline{T}$, which is related to $F_{T'}$ as

$$F_{T'/\overline{T}} = \frac{F_{T'}}{\overline{T}^2},$$
(2)

where $\overline{T}$ is taken to be the mean temperature in the vertical extent of the wave packet. The amplitude of a quasi-monochromatic wave $\hat{T}$ is related to the temperature disturbance power P as
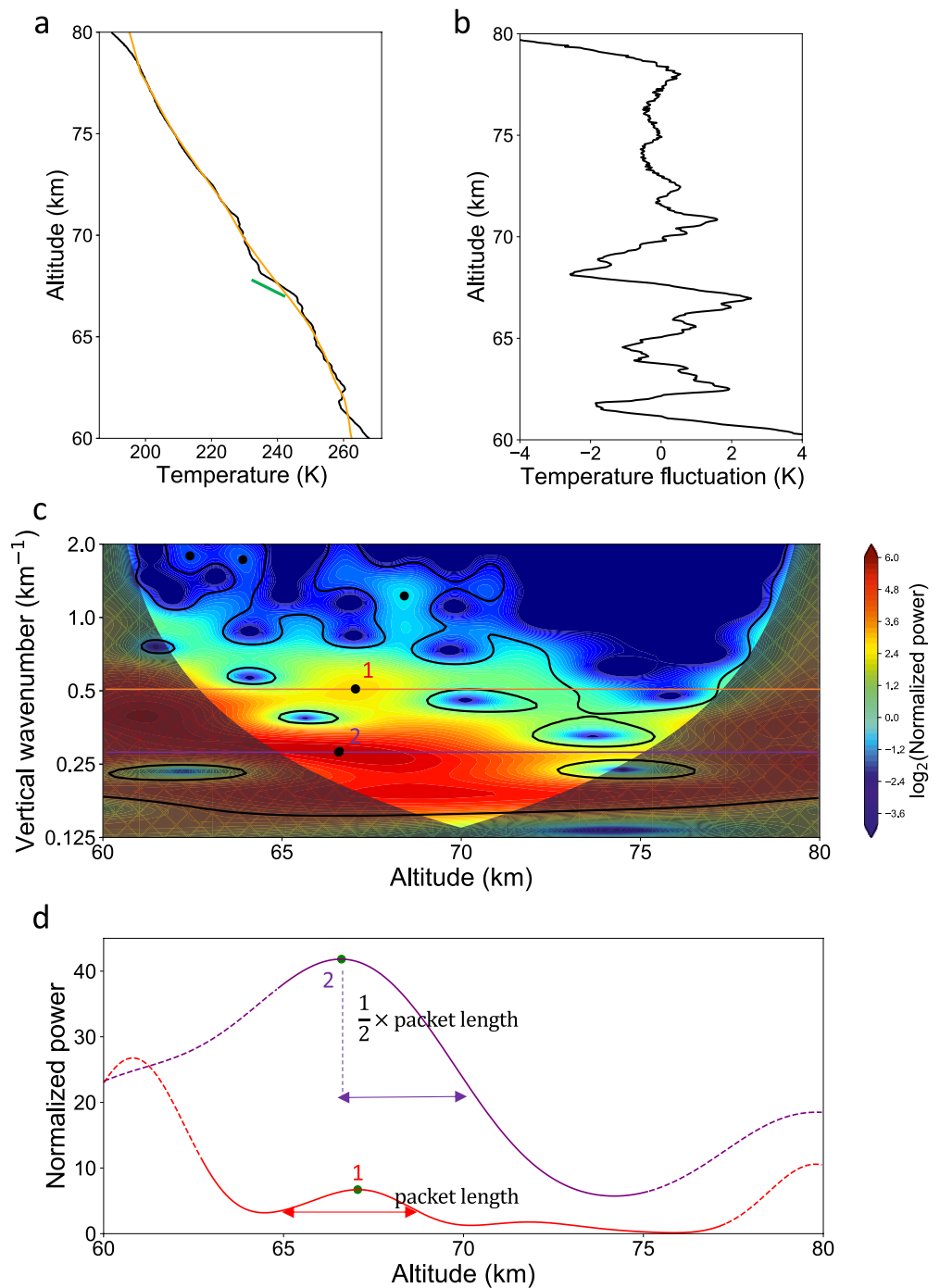
$$P = \frac{\hat{T}^2}{2}.$$
(3)

Figure 2. Example of data processing procedure. The data were obtained by Akatsuki's entry occultation on May 15, 2017 at a latitude of ~20°S. (a) Original temperature profile (black) and smoothed profile obtained by a 4 km-width running average (orange). The green line shows the adiabatic lapse rate of −11.1 K km^{-1}. (b) Residual temperature obtained by subtracting the smoothed profile from the original. (c) Wavelet spectrum of the residual temperature. The colors represent the logarithm to base 2 of the power normalized by the variance, and the solid black lines represent the 90% confidence intervals. The hatched regions represent the cone of influence (COI). The dots indicate the local maxima corresponding to wave packets. (d) Cross sections of the wavelet spectrum along the horizontal lines in panel (c) traversing the local maxima with wavenumbers of ~0.5 km^{-1} (red, indicated by "1") and ~0.3 km^{-1} (purple, indicated by "2"). Cross-sections within the COI are dashed.

Table 1
Numbers of Detected Wave Packets and Numbers of Analyzed Temperature Profiles (in Parentheses) From Venus Express and Akatsuki Radio Occultation Classified According to the Altitude and the Latitude

	Altitude		Latitude	
	60–70 km	70–80 km	<45°	>45°
Venus Express	58 (32)	22 (32)	18 (10)	62 (22)
Akatsuki	43 (27)	10 (27)	40 (20)	13 (7)

P is obtained by integrating the spectral density with respect to the wavenumber. Since the spectral width of a peak for the wavelet transform of a monochromatic wave is determined by the shape of the wavelet basis function and is proportional to the center wavenumber k_z, we can assume a relation:

$$P = \alpha k_z F_{T'}, \quad (4)$$

where α is a nondimensional constant. Then, from (Equations 3 and 4), the amplitude is obtained as

$$\hat{T} = \left(2\alpha k_z F_{T'} \right)^{1/2}. \quad (5)$$

By applying a wavelet transform to monochromatic waves with various wavelengths, it was shown that $\alpha \sim 0.59$ irrespective of the wavelength.

The error in the peak spectral density originates from the background component of the wavelet spectrum, which is comparable to the fluctuation of the background spectral density. This quantity is measured by the standard deviation of the spectral density in the region spanning $\pm \lambda_z$ and $\pm k_z$ centered at the peak, excluding the region inside the half maximum level. The error in the amplitude is calculated from the error in the peak spectral density.

The observed temperature oscillations are assumed to be manifestations of gravity waves. To assess the degree of saturation for individual wave packets, the threshold amplitude at which the wave would cause convective instability is calculated for each wave packet. Letting the background temperature at the altitude z be $\bar{T}(z)$, the condition of neutral stability is written as

$$\frac{d\left(\bar{T} + T' \right)}{dz} = -\frac{g}{c_p}, \quad (6)$$

where g is the gravitational acceleration and c_p is the specific heat at constant pressure. When the temperature disturbance is represented by a monochromatic wave with an amplitude of $\hat{T}$ and a vertical wavelength of λ_z, the condition that the wave causes a marginal stability is obtained from (Equation 6) as

$$\hat{T} = \frac{\lambda_z}{2\pi} \left| \frac{\partial \bar{T}}{\partial z} + \frac{g}{c_p} \right|. \quad (7)$$

The measured amplitude is underestimated due to horizontal smoothing along the raypath of radio occultation. Ignoring the bending of the ray, the length of horizontal averaging is estimated to be ~90 km (Imamura et al., 2018). Applying a 90 km-width moving average to sinusoidal functions with various wavelength, it was shown that the underestimation of the amplitude is <30% for horizontal wavelengths of >200 km. It should be noted that the smoothing effect depends on the propagation direction; it is maximized or minimized when the horizontal propagation is parallel or perpendicular to the raypath, respectively.

3. Results

3.1. Distribution of Wave Packets

We detected 133 wave packets in total in the 59 temperature profiles obtained from the selected Venus Express and Akatsuki radio occultation data described in Section 2.1. The wave packets were classified according to the altitude (60–70 km and 70–80 km) and the latitude (<45° and >45°) and are summarized in Table 1. Venus Express has more observations at higher latitudes than at lower latitudes due to its polar orbit, while Akatsuki has more observations at lower latitudes due to its equatorial orbit.

Figure 3 shows a scatter plot of the vertical wavelength and packet length. The wavelengths are scattered over 0.5–4 km. Many wave packets were
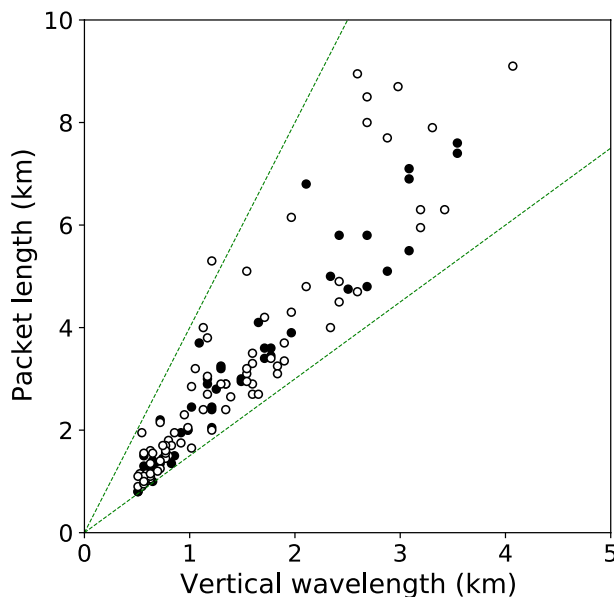

Figure 3. Relationship between the vertical wavelength and the packet length for the Venus Express (open circles) and Akatsuki (filled circles) observations. The green dotted lines indicate slopes of 1.5 and 4.0.
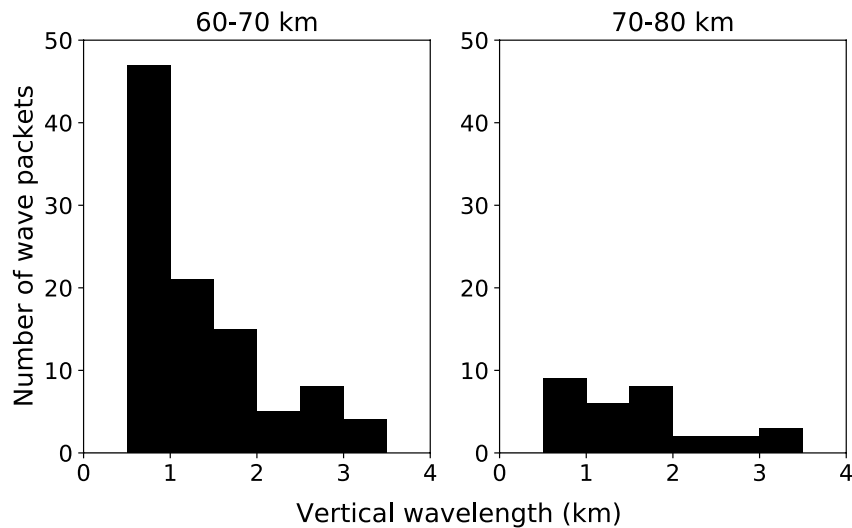
Figure 4. Histograms of the vertical wavelength for the altitude regions of (left) 60–70 km and (right) 70–80 km. The vertical axis is the number of waves occupied by each bin of width 0.5 km.

detected near the short wavelength limit of the analysis, that is, 0.5 km. The dominance of such short wavelength waves have not been previously reported, because of the lower vertical resolution in the previous observations. The packet lengths are distributed over 0.6–10 km. The green dashed lines in Figure 3 show slopes of 1.5 and 4.0, which represent 1.5 and 4.0 cycles per wave packet, respectively. Most of the wave packets are included in this range. The average slope is ~2.2, which means that a wave packet typically includes 2.2 oscillations. Such small numbers of oscillations per packet likely implies transient wave sources such as convection rather than continuous sources such as mountain waves caused by steady surface winds impinging on the topography. The short vertical wavelengths are also difficult to explain by topographic waves, as discussed in Section 4.

The typical number of oscillations per wave packet depends little on the wavelength: it is 2.1, 2.3, 2.4, and 2.1 cycles per wave packet for vertical wavelengths of <1, 1–2, 2–3, and >3 km, respectively. This feature is important for the saturation model as discussed in Section 1 (e.g., Smith et al., 1987). Note that the finite length
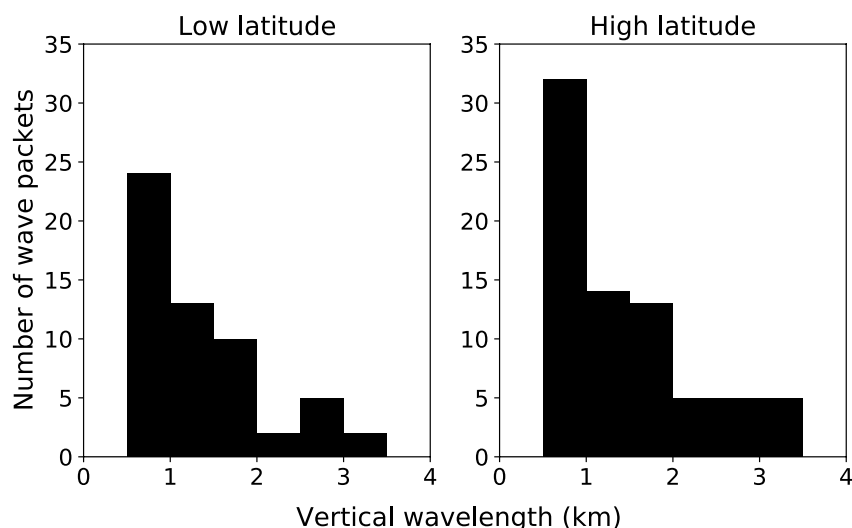

Figure 5. Histograms of the vertical wavelength for the latitude regions of (left) <45° and (right) >45°. The vertical axis is the number of waves occupied by each bin of width 0.5 km.
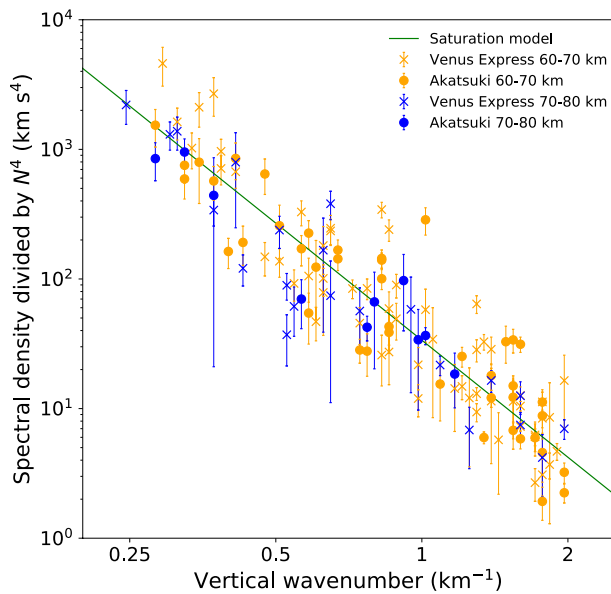
Figure 6. Peak spectral densities of wave packets plotted against vertical wavenumber in the altitude regions of 60–70 km (orange) and 70–80 km (blue), obtained from the measurements by Venus Express (crosses) and Akatsuki (dots). The saturation model is shown for comparison (green line).

Figure 7. Amplitudes of wave packets plotted against vertical wavenumber in the altitude regions of 60–70 km (orange) and 70–80 km (blue), obtained from the measurement by Venus Express (crosses) and Akatsuki (dots).

of the wavelet basis function, which is $\sim$2 cycles for Morlet (Torrence & Compo, 1998), limits the detectable wave packets; the absence of waves below the slope of 1.5 can be attributed to the fact that the wavelet transform is insensitive to wave packets shorter than the width of the wavelet function. This means that the typical number of wave cycles might be underestimated. Nevertheless, oscillations of less than one cycle cannot be regarded as waves, and thus the influence of the width of the wavelet function should be small. There is no systematic difference between the Venus Express and Akatsuki observations.

Figure 4 shows histograms of the vertical wavelength for the two altitude regions. It is remarkable that waves of short vertical wavelengths (<1.5 km) are much more prevalent at lower altitudes than at higher altitudes. This feature is attributed to the preferential dissipation of short vertical wavelength waves through radiative damping in the course of upward propagation (Crisp, 1989; Hinson & Jenkins, 1995). Figure 5 shows the histograms for the two latitude regions, and shows no notable difference.

3.2. Spectral Density and Amplitude

Figure 6 shows the peak spectral densities of the fractional temperature disturbance divided by the fourth power of the Brunt-Väisälä frequency N, that is, $F_{T'/\bar{T}}/N^4$, classified according to the altitude regions and plotted against the vertical wavelength. The saturation model (Equation 1) is also plotted for comparison. It is noteworthy that the spectral densities of the wave packets generally follow the k_z^{-3} power law of the saturation model. Considering that the saturation model is based on a variety of empirically determined parameters (Smith et al., 1987) and that the spectral width of the wavelet spectrum differs from the bandwidth of the wave packet, a quantitative agreement in absolute spectral density is not expected. Nevertheless, it is noteworthy that quasi-monochromatic wave packets collectively reproduce the power law. The typical spectral density at each wavenumber does not clearly depend on the altitude. There is no systematic difference between the Venus Express and Akatsuki observations.
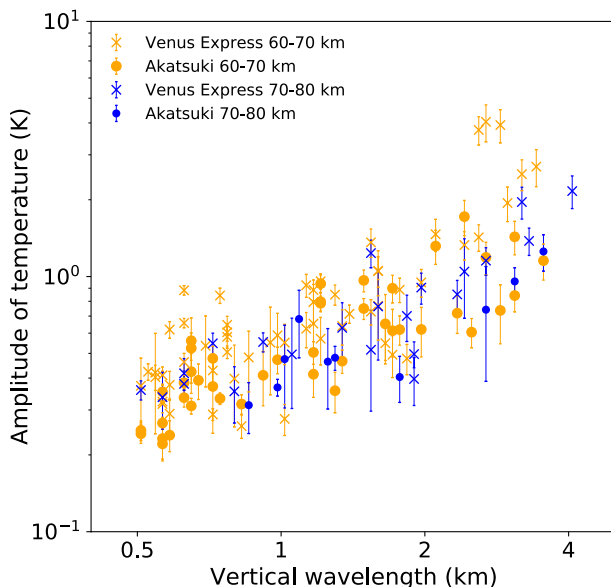
The temperature amplitudes are shown in Figure 7. Waves with longer wavelengths tend to have larger amplitudes, which can be attributed to the larger saturation amplitudes of longer vertical wavelength waves as understood from (Equation 7). The amplitude does not clearly depend on the altitude, although it is slightly larger at lower altitudes. Figure 8 shows the saturation ratio, that is, the ratio of the observed temperature amplitude to the saturation amplitude (Equation 7). The ratio is typically 0.2–0.5 with a mean value of 0.36, consistent with the prediction that the amplitudes are a factor of 3 times smaller than those of individually saturated wave packets (Smith et al., 1987).

The peak spectral densities are classified according to the latitudinal regions in Figure 9, and show no dependence on the latitude. Note, however, that the plotted spectral densities have been divided by N^4, which depends on the latitude. The temperature amplitudes shown in Figure 10 clearly indicate a trend of larger amplitudes at higher latitudes. The saturation ratios shown in Figure 11 do not exhibit a notable latitude dependence. The results are attributed to the fact that the static stability is typically a factor of 2 times higher at high latitudes than at low latitudes above $\sim$60 km altitude (Ando et al., 2020). This tendency
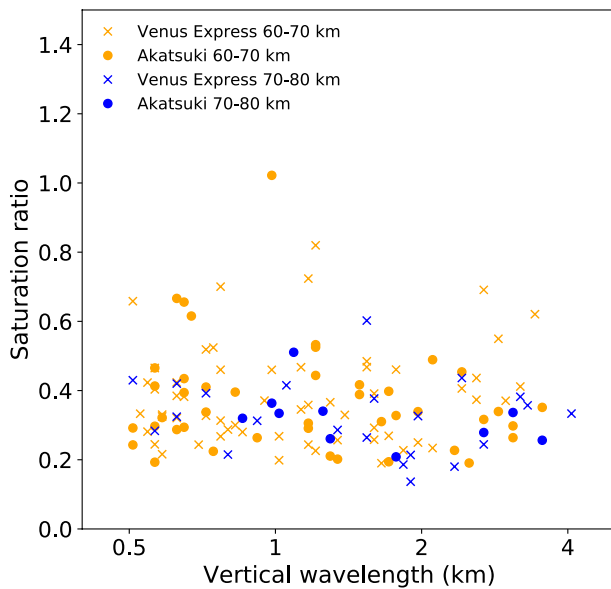
Figure 8. Saturation ratios of wave packets plotted against vertical wavenumber in the altitude regions of 60–70 km (orange) and 70–80 km (blue), obtained from the measurement by Venus Express (crosses) and Akatsuki (dots).

is also seen in the representative static stability profiles shown in Figure 1. N^2 has qualitatively the same latitude dependence. A higher stability means a larger saturation amplitude as implied by (Equation 7), and thus a larger amplitude is allowed at higher latitudes when the saturation ratio is fixed. The spectral densities in Figure 9 are not affected by the change in static stability because they were divided by N^4. This might explain the larger amplitudes of short-vertical scale fluctuations at higher latitudes observed by Venus Express radio occultation (Tellmann et al., 2012) and the stronger radio scintillation at higher latitudes observed by Pioneer Venus radio occultation (Woo et al., 1980). A slight increase of the saturation ratio is seen at high latitudes especially for wavelengths >2 km (Figures 9 and 11), being consistent with the analysis of vertical wavenumber spectra by Ando et al. (2015); more data are needed to confirm the tendency. Imamura et al. (2014) suggested that gravity wave generation by cloud-level convection can be more intense at higher latitudes.

4. Discussion and Conclusions

The characteristics of gravity wave packets seen in vertical temperature profiles of the Venusian atmosphere were studied for the first time. The wavelengths are scattered over 0.5–4.0 km; waves with shorter wavelengths cannot be observed due to the limit of the resolution. The packet lengths are distributed over 0.6–10 km, in which typically 1.5–4.0 oscillations are included. The number of oscillations per wave packet was found to not depend strongly on the wavelength. This result justifies the assumption in the saturation model (Dewan & Good, 1986; Smith et al., 1987) that the bandwidth of each quasi-monochromatic wave is proportional to the wavenumber, which is essential for the k_z^{-3} dependence of the spectral density (see Section 1).
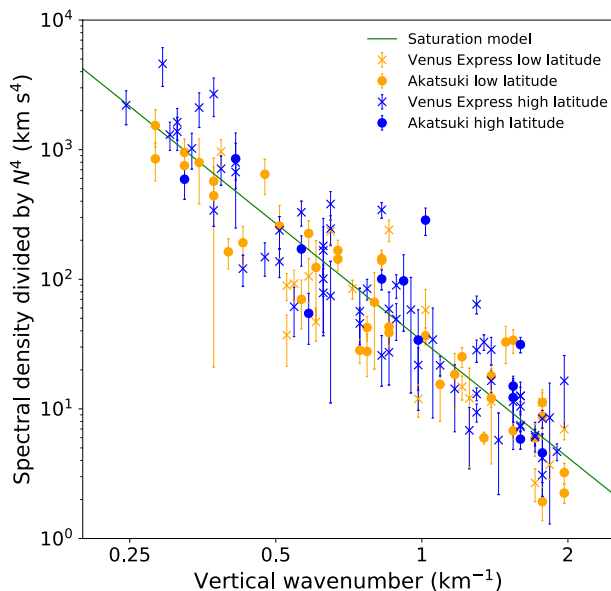
The peak spectral densities of the wave packets are roughly aligned with the k_z^{-3} power law of the saturation model, consistent with the finding that thin neutral layers frequently exist in the Venusian atmosphere (Imamura et al., 2018). This implies that the amplitude of each monochromatic wave is such that the superposition of all waves achieves saturation as predicted by the saturation theory (e.g., Smith et al., 1987). The saturation ratio of each quasi-monochromatic wave is typically 0.2–0.5, which is consistent with the model prediction that the amplitudes are a factor of 3 times smaller than those of individually saturated wave packets. Based on the properties of the wave packets described above, we conclude that the k_z^{-3} power law for the vertical wavenumber spectra observed in the Venusian atmosphere (Ando et al., 2015; Imamura et al., 2018) is a consequence of the superposition of individually unsaturated quasi-monochromatic waves, each of which has a bandwidth proportional to the local wavenumber.

Waves with short vertical wavelengths (<1.5 km) were found to be more prevalent at lower altitudes than at higher altitudes. This might be attributed to radiative damping since the damping rate is higher for short-vertical wavelength waves (Crisp, 1989; Hinson & Jenkins, 1995; Imamura & Ogawa, 1995). The saturated waves lose energy not only via saturation but also via radiative damping, thereby decreasing the efficiency of turbulence generation (Ando et al., 2015). The evaluation of radiative damping requires information on the wave's frequency, which cannot be obtained by radio occultation. Gravity wave-like oscillations have been observed

Figure 9. Peak spectral densities of wave packets plotted against vertical wavenumber in the latitude regions <45° (orange) and >45° (blue), obtained from the measurements by Venus Express (crosses) and Akatsuki (dots). The saturation model is shown for comparison (green line).
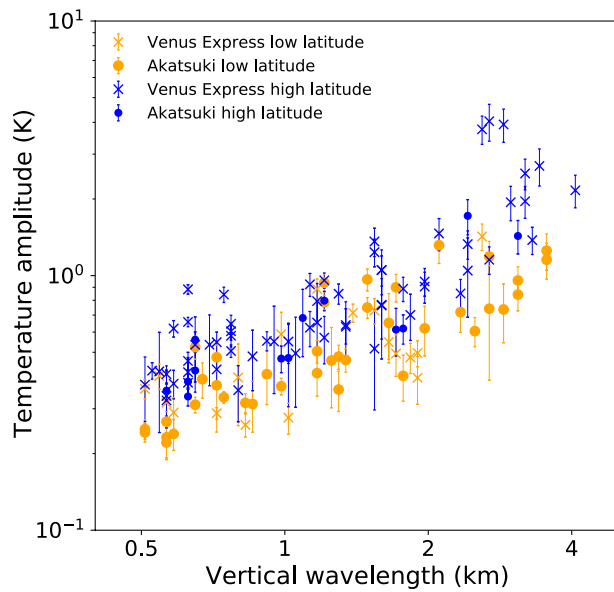
Figure 10. Amplitudes of wave packets plotted against vertical wavenumber in the latitude regions <45° (orange) and >45° (blue), obtained from the measurements by Venus Express (crosses) and Akatsuki (dots).

in the thermosphere (Garcia et al., 2009; Müller-Wodarg et al., 2016); the change in wave characteristics associated with upward propagation into the thermosphere when subjected to radiative damping will be a subject of a future study.

The temperature amplitude is larger at higher latitudes, while no notable latitudinal dependence is found in the saturation ratio and the spectral density divided by N^4. This result is attributed to the increase of the Brunt-Väisälä frequency at high latitudes (Ando et al., 2020), which allows larger saturation amplitudes at higher latitudes. This might explain the high-latitude enhancement of short-vertical scale fluctuations seen in radio occultation temperatures (Ando et al., 2015; Tellmann et al., 2012), although the latitudinal variation of gravity wave sources cannot be ruled out since a slight increase of the saturation ratio is seen at high latitudes especially for wavelengths >2 km. The higher scintillation power at higher latitudes observed in the Pioneer Venus radio occultation (Woo et al., 1980) might also result from the large saturation amplitude at high latitudes, since the density fluctuation responsible for the scintillation should be larger for larger temperature fluctuations. The idea that the amplitudes of gravity waves can be mostly determined by the background stability will lead to an improvement of the parameterization of the wave momentum flux and the wave-induced eddy diffusivity in general circulation models of the planets (Medvedev et al., 2011; Yiğit et al., 2008; Zalucha et al., 2013).

Although similar wavenumber spectra were seen in the Earth's and Venusian atmospheres, the process determining the wavenumber spectrum is debatable (Ando et al., 2015). The spectrum might be affected by interactions among different wavenumbers (Dewan, 1997; Hines, 1991; Weinstock, 1985). Radiative damping that is stronger at higher wavenumbers can also cause a power-law dependence (Zhu, 1994). The apparent universality of the spectrum across the planets that have different atmospheric conditions will be helpful in constraining the mechanism. Ando et al. (2012) studied radio occultation temperatures of the Martian atmosphere obtained by conventional geometrical optics and found a similar power-law dependence. A wavelet analysis of high-vertical-resolution profiles obtained by the radio holographic method for the Martian atmosphere will be performed in the future. A comparison with the temperature fluctuations in Saturn's atmosphere obtained by stellar occultation, for which Harrington et al. (2010) showed a vertical wavenumber spectrum indicating saturation, would also provide clues.
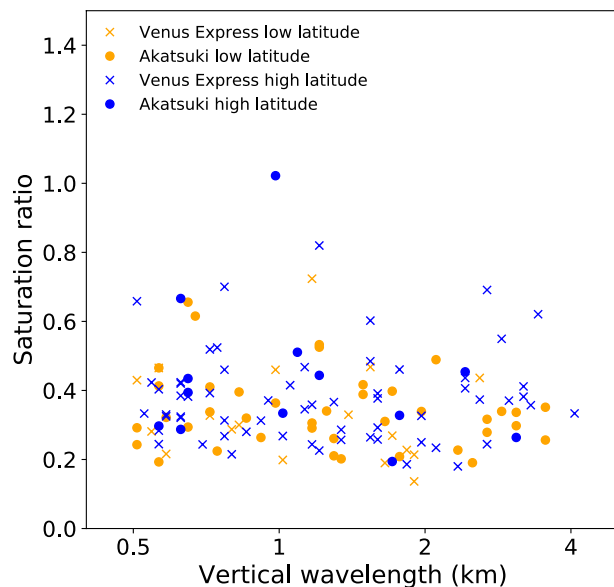
The fact that each wave packet includes only a few oscillations implies that the waves are generated by transient sources such as convection and the meandering motion of jets. The observed short vertical wavelengths also make it unlikely that topographic gravity waves constitute the wave packets; because of the large intrinsic phase speeds due to the superrotation of the atmosphere (Sánchez-Lavega et al., 2017; Schubert et al., 1980), the vertical wavelengths of topographic gravity waves should be >10 km (Lefèvre et al., 2019; Yamada et al., 2019). Gravity wave generation by cloud-level convection has been studied using mesoscale numerical models (Imamura et al., 2014; Lefè vre et al., 2017, 2018). A three-dimensional model with vertical shear by Lefè vre et al. (2018) reproduced gravity waves with amplitudes of ~1.5 K around 60 km altitude, comparable to the observations. However, the wave characteristics at higher altitudes are unclear, and furthermore, a much wider model domain and higher vertical resolution are needed to reproduce wavenumber spectra that can

Figure 11. Saturation ratios of wave packets plotted against vertical wavenumber in the latitude regions <45° (orange) and >45° (blue), obtained from the measurements by Venus Express (crosses) and Akatsuki (dots).

be compared with the observations. Other possible sources are transient large-scale motions associated with barotropic/baroclinic instability (Lebonnois et al., 2016; Sugimoto et al., 2014) and shear instability (Imamura, 1997). Comprehensive studies combining high-resolution dynamical models and wavelet analyses of radio occultation temperatures and cloud images are needed to identify the wave sources.

No notable difference was found between the Venus Express and Akatsuki observations, which are separated by ~10 years from each other, although long-term variations in the mean zonal velocity at cloud heights and the ultraviolet albedo have been reported (Horinouchi et al., 2018; Khatuntsev et al., 2013; Kouyama et al., 2013; Lee et al., 2019; Peralta et al., 2018; Rossow et al., 1990). This may suggest that the gravity wave activity is not sensitive to such variations. To confirm the tendency and constrain the interaction between gravity waves and the background atmospheric structure, more data including those taken in the latter half of the Venus Express mission and taken after 2017 in the Akatsuki mission should be analyzed.

Data Availability Statement

The radio science data used in this study are available at Planetary Data System (PDS) of NASA (under the heading "VRA" on https://pds-atmospheres.nmsu.edu/ve/) and Data ARchives and Transmission System (DARTS) of JAXA (Murakami et al., 2017) (https://doi.org/10.17597/ISAS.DARTS/VCO-00014). The temperature profiles derived from the radio science data with radio holographic method are given at Zenodo (Imamura, 2021) (https://doi.org/10.5281/zenodo.5106343).

References

Ando, H., Imamura, T., Tellmann, S., Pätzold, M., Häusler, B., Sugimoto, N., et al. (2020). Thermal structure of the Venusian atmosphere from the sub-cloud region to the mesosphere as observed by radio occultation. *Scientific Reports*, *10*, 3448. https://doi.org/10.1038/s41598-020-59278-8

Ando, H., Imamura, T., & Tsuda, T. (2012). Vertical wavenumber spectra of gravity waves in the Martian atmosphere obtained from Mars Global Surveyor radio occultation data. *Journal of the Atmospheric Sciences*, *69*, 2906–2912. https://doi.org/10.1175/JAS-D-11-0339.1

Ando, H., Imamura, T., Tsuda, T., Tellmann, S., Pätzold, M., & Häusler, B. (2015). Vertical wavenumber spectra of gravity waves in the Venus atmosphere obtained from Venus Express radio occultation data: Evidence for saturation. *Journal of the Atmospheric Sciences*, *6*, 2318–2329. https://doi.org/10.1175/jas-d-14-0315.1

Crisp, D. (1989). Radiative forcing of the Venus mesosphere. II. Thermal fluxes, cooling rates, and radiative equilibrium temperatures. *Icarus*, *77*, 391–413. https://doi.org/10.1016/0019-1035(89)90096-1

Dewan, E. M. (1997). Saturated-cascade similitude theory of gravity wave spectra. *Journal of Geophysical Research*, *102*, 29799–29817. https://doi.org/10.1029/97JD02151

Dewan, E. M., & Good, R. E. (1986). Saturation and the "universal" spectrum for vertical profiles of horizontal scalar winds in the atmosphere. *Journal of Geophysical Research*, *91*, 2742–2748. https://doi.org/10.1029/jd091id02p02742

Fritts, D. C., & Alexander, M. J. (2003). Gravity wave dynamics and effects in the middle atmosphere. *Reviews of Geophysics*, *41*(1), 1003. https://doi.org/10.1029/2001RG000106

Fukuhara, T., Futaguchi, T., Hashimoto, G. L., Horinouchi, T., Imamura, T., Iwagami, N., et al. (2017). Large stationary gravity wave in the atmosphere of Venus. *Nature Geoscience*, *10*(2), 85–88. https://doi.org/10.1038/ngeo2873

Garcia, R. F., Drossart, P., Piccioni, G., López-Valverde, M., & Occhipinti, G. (2009). Gravity waves in the upper atmosphere of Venus revealed by CO_2 nonlocal thermodynamic equilibrium emissions. *Journal of Geophysical Research*, *114*, E00B32. https://doi.org/10.1029/2008JE003073

Harrington, J., French, R. G., & Matcheva, K. (2010). The 1998 November 14 occultation of GSC 0622-00345 by Saturn. II. Stratospheric thermal profile, power spectrum, and gravity waves. *The Astrophysical Journal*, *716*, 404–416. https://doi.org/10.1088/0004-637x/716/1/404

Häusler, B., Pätzold, M., Tyler, G. L., Simpson, R. A., Bird, M. K., Dehant, V., et al. (2006). Radio science investigations by VeRa onboard the Venus Express spacecraft. *Planetary and Space Science*, *54*(13–14), 1315–1335. https://doi.org/10.1016/j.pss.2006.04.032

Hines, C. O. (1991). The saturation of gravity waves in the middle atmosphere. Part II: Development of Doppler-spread theory. *Journal of the Atmospheric Sciences*, *48*, 1360–1379. https://doi.org/10.1175/1520-0469(1991)048,1361:TSOGWI.2.0.CO;2

Hinson, D. P., & Jenkins, J. M. (1995). Magellan radio occultation measurements of atmospheric waves on Venus. *Icarus*, *114*, 310–327. https://doi.org/10.1006/icar.1995.1064

Horinouchi, T., Kouyama, T., Lee, Y. J., Murakami, S., Ogohara, K., Takagi, M., et al. (2018). Mean winds at the cloud top of Venus obtained from two-wavelength UV imaging by Akatsuki. *Earth Planets and Space*, *70*, 10. https://doi.org/10.1186/s40623-017-0775-3

Hoshino, N., Fujiwara, H., Takagi, M., & Kasaba, Y. (2013). Effects of gravity waves on the day-night difference of the general circulation in the Venusian lower thermosphere. *Journal of Geophysical Research*, *118*, 2004–2015. https://doi.org/10.1002/jgre.20154

Hou, A. Y., & Farrell, B. F. (1987). Superrotation induced by critical-level absorption of gravity waves on Venus: An assessment. *Journal of the Atmospheric Sciences*, *44*, 1049–1061.

Imamura, T. (1997). Momentum balance of the Venusian midlatitude mesosphere. *Journal of Geophysical Research*, *102*, 6615–6620. https://doi.org/10.1029/96je03882

Imamura, T. (2021). *Vertical temperature profiles obtained from Venus Express and Akatsuki radio occultation data using FSI [Data set]*. Zenodo. https://doi.org/10.5281/zenodo.5106343

Imamura, T., Ando, H., Tellmann, S., Pätzold, M., Häusler, B., Yamazaki, A., et al. (2017). Initial performance of the radio occultation experiment in the Venus orbiter mission Akatsuki. *Earth Planets and Space*, *69*, 137. https://doi.org/10.1186/s40623-017-0722-3

Imamura, T., Higuchi, T., Maejima, Y., Takagi, M., Sugimoto, N., Ikeda, K., & Ando, H. (2014). Inverse insolation dependence of Venus' cloud-level convection. *Icarus*, *228*, 181–188. https://doi.org/10.1016/j.icarus.2013.10.012

Imamura, T., Miyamoto, M., Ando, H., Häusler, B., Pätzold, M., Tellmann, S., et al. (2018). Fine vertical structures at the cloud heights of Venus revealed by radio holographic analysis of Venus Express and Akatsuki radio occultation data. *Journal of Geophysical Research*, *123*. https://doi.org/10.1029/2018JE005627

Imamura, T., & Ogawa, T. (1995). Radiative damping of gravity waves in the terrestrial planetary atmospheres. *Geophysical Research Letters*, *22*, 267–270. https://doi.org/10.1029/94gl02998

Ingersoll, A. P., Crisp, D., Grossman, A. W., & VEGA Balloon Science Team. (1987). Estimates of convective heat fluxes and gravity wave amplitudes in the Venus middle cloud layer from VEGA balloon measurements. *Advances in Space Research*, *7*(12), 343–349. https://doi.org/10.1016/0273-1177(87)90242-0

Jensen, A. S., Lohmann, M. S., Benzon, H. H., & Nielsen, A. S. (2003). Full Spectrum Inversion of radio occultation signals. *Radio Science*, *38*, 1040. https://doi.org/10.1029/2002RS002763

Khatuntsev, I. V., Patsaeva, M. V., Titov, D. V., Ignatiev, N. I., Turin, A. V., Limaye, S. S., et al. (2013). Cloud level winds from the Venus express monitoring camera imaging. *Icarus*, *226*, 140–158. https://doi.org/10.1016/j.icarus.2013.05.018

Kitahara, T., Imamura, T., Sato, T. M., Yamazaki, A., Lee, Y. J., Yamada, M., et al. (2019). Stationary features at the cloud top of Venus observed by Ultraviolet Imager onboard Akatsuki. *Journal of Geophysical Research: Planets*, *124*, 1266–1281. https://doi.org/10.1029/2018JE005842

Kouyama, T., Imamura, T., Nakamura, M., Satoh, T., & Futaana, Y. (2013). Long-term variation in the cloud-tracked zonal velocities at the cloud top of Venus deduced from Venus Express VMC images. *Journal of Geophysical Research*, *118*, 37–46. https://doi.org/10.1029/2011JE004013

Kouyama, T., Imamura, T., Taguchi, M., Fukuhara, T., Sato, T. M., Yamazaki, A., et al. (2017). Topographical and local time dependence of large stationary gravity waves observed at the cloud top of Venus. *Geophysical Research Letters*, *44*, 12098–12105. https://doi.org/10.1002/2017GL075792

Lebonnois, S., Sugimoto, N., & Gilli, G. (2016). Wave analysis in the atmosphere of Venus below 100-km altitude, simulated by the LMD Venus GCM. *Icarus*, *278*, 38–51. https://doi.org/10.1016/j.icarus.2016.06.004

Lee, Y. J., Jessup, K.-L., Perez-Hoyos, S., Titov, D. V., Lebonnois, S., Peralta, J., et al. (2019). Long-term variations of Venus' 365-nm albedo observed by Venus Express, Akatsuki, MESSENGER, and Hubble Space Telescope. *The Astronomical Journal*, *158*, 126. https://doi.org/10.3847/1538-3881/ab3120

Lefèvre, M., Lebonnois, S., & Spiga, A. (2018). Three-dimensional turbulence-resolving modeling of the Venusian cloud layer and induced gravity waves: Inclusion of complete radiative transfer and wind shear. *Journal of Geophysical Research*, *123*, 2773–2789. https://doi.org/10.1029/2018JE005679

Lefèvre, M., Spiga, A., & Lebonnois, S. (2017). Three-dimensional turbulence-resolving modeling of the Venusian cloud layer and induced gravity waves. *Journal of Geophysical Research*, *122*, 134–149. https://doi.org/10.1002/2016JE005146

Lefèvre, M., Spiga, A., & Lebonnois, S. (2019). Mesoscale modeling of Venus' bow-shape waves. *Icarus*, *335*, 113376.

Lindzen, R. S. (1981). Turbulence and stress owing to gravity and tidal breakdown. *Journal of Geophysical Research*, *86*, 9707–9714. https://doi.org/10.1029/jc086ic10p09707

Medvedev, A. S., Yigit, E., Hartogh, P., & Becker, E. (2011). Influence of gravity waves on the Martian atmosphere: General circulation modeling. *Journal of Geophysical Research*, *116*, E10004. https://doi.org/10.1029/2011JE003848

Müller-Wodarg, I. C. F., Ingo, C. F., Bruinsma, S., Marty, J.-C., & Svedhem, H. (2016). In situ observations of waves in Venus's polar lower thermosphere with Venus Express aerobraking. *Nature Physics*, *12*, 767–771. https://doi.org/10.1038/nphys3733

Murakami, S., Ando, H., Imamura, T., Yamamoto, Y., & Hashimoto, G. L. (2017). *Venus climate orbiter Akatsuki RS Doppler profiles PDS3 dataset (1.0) [Data set]*. Institute of Space and Astronautical Science, Japan Aerospace Exploration Agency. https://doi.org/10.17597/ISAS.DARTS/VCO-00014

Nakamura, M., Imamura, T., Ishii, N., Abe, T., Kawakatsu, Y., Hirose, C., et al. (2016). AKATSUKI returns to Venus. *Earth Planets and Space*, *68*, 75. https://doi.org/10.1186/s40623-016-0457-6

Nakamura, M., Imamura, T., Ishii, N., Abe, T., Satoh, T., Suzuki, M., et al. (2011). Overview of Venus orbiter, Akatsuki. *Earth Planets and Space*, *63*, 443–457. https://doi.org/10.5047/eps.2011.02.009

Peralta, J., Hueso, R., Sánchez-Lavega, A., Piccioni, G., Lanciano, O., & Drossart, P. (2008). Characterization of mesoscale gravity waves in the upper and lower clouds of Venus from VEX-VIRTIS images. *Journal of Geophysical Research*, *113*, E00B18. https://doi.org/10.1029/2008JE003185

Peralta, J., Muto, K., Hueso, R., Horinouchi, T., Sánchez-Lavega, A., Murakami, S.-y., et al. (2018). Nightside winds at the lower clouds of Venus with Akatsuki/IR2: Longitudinal, local time, and decadal variations from comparison with previous measurements. *The Astrophysical Journal Supplement Series*, *239*, 29. https://doi.org/10.3847/1538-4365/aae844

Peralta, J., Sánchez-Lavega, A., Horinouchi, T., McGouldrick, K., Garate-Lopez, I., Young, E. F., et al. (2019). New cloud morphologies discovered on the Venus's night during Akatsuki. *Icarus*, *333*, 177–182. https://doi.org/10.1016/j.icarus.2019.05.026

Piccialli, A., Titov, D. V., Sánchez-Lavega, A., Peralta, J., Shalygina, O., Markiewicz, W. J., & Svedhem, H. (2014). High latitude gravity waves at the Venus cloud tops as observed by the Venus Monitoring Camera on board Venus Express. *Icarus*, *227*, 94–111. https://doi.org/10.1016/j.icarus.2013.09.012

Rossow, W. B., Del Genio, A. D., & Eichler, T. (1990). Cloud-tracked winds from Pioneer Venus OCPP images. *Journal of the Atmospheric Sciences*, *47*, 2053–2084. https://doi.org/10.1175/1520-0469(1990)047<2053:CTWFVO>2.0.CO;2

Sánchez-Lavega, A., Lebonnois, S., Imamura, T., Read, P., & Luz, D. (2017). The atmospheric dynamics of Venus. *Space Science Reviews*, *212*, 1541–1616. https://doi.org/10.1007/s11214-017-0389-x

Sato, K., & Yamada, M. (1994). Vertical structure of atmospheric gravity waves revealed by the wavelet analysis. *Journal of Geophysical Research*, *99*, 20623–20631. https://doi.org/10.1029/94jd01818

Sato, T. M., Satoh, T., Sagawa, H., Manago, N., Lee, Y. J., Murakami, S., et al. (2020). Dayside cloud top structure of Venus retrieved from Akatsuki IR2 observations. *Icarus*, *345*, 113682. https://doi.org/10.1016/j.icarus.2020.113682

Schubert, G., Covey, C., Genio, A. D., Elson, L. S., Keating, G., Seiff, A., et al. (1980). Structure and circulation of the Venus atmosphere. *Journal of Geophysical Research*, *85*, 8007–8025. https://doi.org/10.1029/ja085ia13p08007

Schubert, G., & Walterscheid, R. L. (1984). Propagation of small-scale acoustic-gravity waves in the Venus atmosphere. *Journal of the Atmospheric Sciences*, *41*, 1202–1213. https://doi.org/10.1175/1520-0469(1984)041<1202:possag>2.0.co;2

Seiff, A., Schofield, J. T., Kliore, A. J., Taylor, F. W., Limaye, S. S., Revercomb, H. E., et al. (1985). Models of the structure of the atmosphere of Venus from the surface to 100 kilometers altitude. *Advances in Space Research*, *5*, 3–58. https://doi.org/10.1016/0273-1177(85)90197-8

Seiff, A., Young, R. E., Haberle, R., & Houben, H. (1992). The evidences of waves in the atmospheres of Venus and Mars. In J. G. Luhmann, M. Tatrallyay, & R. O. Pepin (Eds.), *Venus and Mars: Atmospheres, ionospheres, and solar wind interactions* (pp. 73–89). American Geophysical Union.

Shimomai, T., Yamanaka, M. D., & Fukao, S. (1996). Application of wavelet analysis to wind disturbances observed with MST radar techniques. *Journal of Atmospheric and Terrestrial Physics*, *58*, 683–696. https://doi.org/10.1016/0021-9169(95)00067-4

Smith, S. A., Fritts, D. C., & VanZandt, T. E. (1987). Evidence of a saturation spectrum of atmospheric gravity waves. *Journal of the Atmospheric Sciences*, *44*, 1404–1410. https://doi.org/10.1175/1520-0469(1987)044<1404:efasso>2.0.co;2

Sugimoto, N., Takagi, M., & Matsuda, Y. (2014). Baroclinic instability in the Venus atmosphere simulated by GCM. *Journal of Geophysical Research*, *119*, 1950–1968. https://doi.org/10.1002/2014JE004624

Svedhem, H., Titov, D. V., McCoy, D., Lebreton, J.-P., Barabash, S., Bertaux, J.-L., et al. (2007). Venus Express—The first European mission to Venus. *Planetary and Space Science*, *55*, 1636–1652. https://doi.org/10.1016/j.pss.2007.01.013

Tellmann, S., Häusler, B., Hinson, D. P., Tyler, G. L., Andert, T. P., Bird, M. K., et al. (2012). Small-scale temperature fluctuations seen by the VeRa Radio Science Experiment on Venus Express. *Icarus*, *221*(2), 471–480. https://doi.org/10.1016/j.icarus.2012.08.023

Tellmann, S., Pätzold, M., Häusler, B., Bird, M. K., & Tyler, G. L. (2009). Structure of the Venus neutral atmosphere as observed by the Radio Science experiment VeRa on Venus Express. *Journal of Geophysical Research*, *114*, E00B36. https://doi.org/10.1029/2008JE003204

Torrence, C., & Compo, G. P. (1998). A practical guide to wavelet analysis. *Bulletin of the American Meteorological Society*, *79*, 61–78. https://doi.org/10.1175/1520-0477(1998)079<0061:apgtwa>2.0.co;2

Tsuda, T., & Hocke, K. (2002). Vertical wave number spectrum of temperature fluctuations in the stratosphere using GPS occultation data. *Journal of the Meteorological Society of Japan*, *80*, 925–938. https://doi.org/10.2151/jmsj.80.925

Tsuda, T., Inoue, T., Fritts, D. C., VanZandt, T. E., Kato, S., Sato, T., & Fukao, S. (1989). MST radar observations of a saturated gravity wave spectrum. *Journal of the Atmospheric Sciences*, *46*, 2440–2447. https://doi.org/10.1175/1520-0469(1989)046<2440:mrooas>2.0.co;2

Tsuda, T., Lin, X., Hayashi, H., & Noersomadi, N. (2011). Analysis of vertical wave number spectrum of atmospheric gravity waves in the stratosphere using COSMIC GPS radio occultation data. *Atmospheric Measurement Techniques*, *4*, 1627–1636. https://doi.org/10.5194/amt-4-1627-2011

Tsuda, T., VanZandt, T. E., Mizumoto, M., Kato, S., & Fukao, S. (1991). Spectral analysis of temperature and Brunt-Vaisala frequency fluctuations observed by radiosondes. *Journal of Geophysical Research*, *96*, 17265–17278. https://doi.org/10.1029/91jd01944

Weinstock, J. (1985). Theoretical gravity wave spectrum in the atmosphere: Strong and weak wave interactions. *Radio Science*, *20*, 1295–1300. https://doi.org/10.1029/RS020i006p01295

Woo, R., Armstrong, J. W., & Ishimaru, A. (1980). Radio occultation measurements of turbulence in the Venus atmosphere by Pioneer Venus. *Journal of Geophysical Research*, *85*, 8031–8038. https://doi.org/10.1029/ja085ia13p08031

Yamada, T., Imamura, T., Fukuhara, T., & Taguchi, M. (2019). Influence of the cloud-level neutral layer on the vertical propagation of topographically generated gravity waves on Venus. *Earth Planets and Space*, *71*, 123. https://doi.org/10.1186/s40623-019-1106-7

Yiğit, E., Aylward, A. D., & Medvedev, A. S. (2008). Parameterization of the effects of vertically propagating gravity waves for thermosphere general circulation models: Sensitivity study. *Journal of Geophysical Research*, *113*, D19106. https://doi.org/10.1029/2008JD010135

Zalucha, A. M., Brecht, A. S., Rafkin, S., Bougher, S. W., & Alexander, M. J. (2013). Incorporation of a gravity wave momentum deposition parameterization into the Venus thermosphere general circulation model (VTGCM). *Journal of Geophysical Research*, *118*, 147–160. https://doi.org/10.1029/2012JE004168

Zhu, X. (1994). A new theory of the saturated gravity wave spectrum for the middle atmosphere. *Journal of the Atmospheric Sciences*, *51*, 3615–3626. https://doi.org/10.1175/1520-0469(1994)051,3615:ANTOTS.2.0.CO;2